



Alumina effect on the structure and properties of calcium aluminosilicate in the percalcic region: A molecular dynamics investigation

Achraf Atila^{a,b,**}, El Mehdi Ghardi^a, Abdellatif Hasnaoui^{c,*}, Said Ouaskit^a

^a Laboratoire physique de la matière condensée, Faculté des sciences Ben M'sik, Université Hassan II de Casablanca, Morocco

^b Department of Materials Science and Engineering, Institute I, Friedrich-Alexander-Universität Erlangen-Nürnberg (FAU), Martensstr. 5, Erlangen 91058, Germany

^c LS3M, Faculté Polydisciplinaire Khouribga, University Sultan Moulay Slimane, B.P 145, 25000 Khouribga, Morocco

ARTICLE INFO

Keywords:

Elastic properties
Glass transition
Calcium aluminosilicate
Aluminium avoidance parameter
Molecular dynamics

ABSTRACT

We rely on molecular dynamics simulations to investigate and discuss the effect of alumina content on the thermodynamic, elastic and structural properties of calcium aluminosilicate glasses in the light of available experimental data. The alumina content varies from low to intermediate ranges by considering compositions of $(CaO - SiO_2)_{(1-x)}(Al_2O_3)_x$ where $x = 0-30$ mol%. The glass transition temperature was found by referring to the concept of inherent structure energy while elastic properties were computed using two methods: the first is via molecular statics using energy minimization and the second one by performing molecular dynamics at a finite temperature. We suggest a correlation between structural changes, mechanical properties and glass transition temperature, through an analysis of the short and medium range orders. The results show that by increasing Al_2O_3 content, an increase in the population of bridging oxygens and oxygen tricluster is observed while free oxygens tend to vanish. Regions with rich $Al-O-Al$ linkages start to appear as shown by the aluminium avoidance parameter, which is also accompanied with an increase of the glass transition temperature and elastic moduli.

1. Introduction

In the last decades, new and very high request has evolved for innovative approaches toward stronger or, more precisely, more damage and crack resistant glasses [1]. The improvement of strength, toughness, and elastic properties of glass are now a main challenge for further progress in the development of new glasses with superior properties to meet the our needs for various industrial, technological, and clinical applications [2,3].

Increasing the strength and toughness of glass would not only allow interesting new applications, but also lead to a major reduction of material investment for existing applications. In this respect, and generally speaking, silicate-based glasses and their properties (e.g. thermodynamic, mechanical) are usual topics of studies in condensed matter physics, glass science and material physics and chemistry. These materials were studied both theoretically and experimentally as a fundamental and complex problem [4,5]. In the last years, numerous

reports on binary glasses of calcium silicate $CaO - SiO_2$ [6] (CS), calcium aluminate $CaO - Al_2O_3$ [7] and ternary glasses of calcium aluminosilicate $CaO - Al_2O_3 - SiO_2$ [8,9] (CAS) have been undertaken to study the properties of these type of materials.

Basically, the structure of silica glass is usually formed by a continuous network of SiO_4 tetrahedra connected by bridging oxygens (BOs^1), as has been shown by the random network model [10]. The addition of alkali or alkaline-earth atoms results in a depolymerization of the glass network, by transforming the BOs to non-bridging oxygens ($NBOs^2$) and to free oxygens (FO) and sometimes to oxygen triclusters TBOs in the case of alkali and alkaline-earth aluminosilicates.

The glass network can be described by tetrahedral units known as Q^n , where n stands for the number of bridging oxygens in each network former polyhedra. This provides information on the number of bridging oxygens and then on the degree of network polymerization.

The addition of aluminium in this type of network significantly changes the structure, and by the presence of M-modifying ions (M

* Corresponding author.

** Corresponding author at: Department of Materials Science and Engineering, Institute I, Friedrich-Alexander-Universität Erlangen-Nürnberg (FAU), Martensstr. 5, Erlangen 91058, Germany

E-mail addresses: achraf.atila@fau.de (A. Atila), hasnaoui59@hotmail.com (A. Hasnaoui).

¹ Bridging oxygens (BOs) are oxygens that are linked to two network formers (Si and/or Al).

² Non-bridging oxygens (NBOs) are oxygens that are linked to at least one network modifier atom (Ca in this case).

denotes Ca in our case), aluminium is preferentially inserted in tetrahedral positions forming negatively charged units AlO_4^- . We observe then the formation of $Al-O-Si$ bonds. These bonds are energetically more favourable than $Si-O-Si$ and $Al-O-Al$ bonds according to the Loewenstein principle [11,12].

The representative image of aluminosilicate glasses is an interpenetration of the two-tetrahedral networks formed by Si and Al . The tetrahedral network consists essentially of SiO_4 and AlO_4 tetrahedra connected by a BOs. The introduction of Ca into this network, leads to the formation of NBOs in the network by breaking $Si-O-Si$, $Al-O-Al$ and/or $Si-O-Al$ bonds. Thus, calcium plays a role of network modifier. Moreover, the presence of the calcium in the network ensures the charge balancing of the system. The presence of NBOs therefore alters the structure of the calcium aluminosilicate, which has an impact on structural and thermodynamic properties of the glass [13]. In addition, we can also see to the formation of tri-coordinated oxygens (triclusters), which are defined as one oxygen bonded to three network formers. These triclusters are mainly formed from the interaction of two bonded oxygen with Ca modifier cations, while a part of NBO is consumed to produce AlO_5 units as proposed by Stebbins et al. [14].

The distribution of aluminium species depends on the type and content of modifiers (Ca) added to the glass network, and more precisely on the concentration ratio $[CaO]/[Al_2O_3]$. The distribution of Al tetrahedra AlO_4^- , 5-coordinated AlO_5^{2-} and hexahedra AlO_6^{3-} will then depend on the ratio $[CaO]/[Al_2O_3]$

- When the concentration ratio $[CaO]/[Al_2O_3] > 1$, the glass is called percalcic. There is an excess of modifiers compared to alumina. In this case, Al^{3+} ions are essentially present in 4-coordinated configuration AlO_4^- and their charges are compensated by Ca^{2+} cations. In this case, aluminium plays the role of a network former, as shown by Raman spectroscopy studies [15].
- In the case where $[CaO]/[Al_2O_3] = 1$, all Ca^{2+} ions compensate the charges generated by AlO_4^- tetrahedra, which corresponds to a compensation line on which aluminium tectosilicate is located. These glasses are supposed to be completely polymerized and can no longer have NBO [16].
- In the case where $[CaO]/[Al_2O_3] < 1$, the glasses are called peraluminous. They have an excess of modifiers compared to alumina. Al^{3+} ions are compensated by the modifiers are predominantly in 4-coordinated configuration AlO_4^- . The remainder of the aluminium excess with respect to Ca^{2+} ions are inserted into the vitreous network in 5-coordinated AlO_5^{2-} and 6-coordinated AlO_6^{3-} forms.

The present work aims to investigate the effect of alumina content on thermodynamic, elastic and structural properties of $(CaO-SiO_2)_{1-x}(Al_2O_3)_x$ in which the alumina content x can be varied from the calcium silicate (CS) binary glass to CAS with 30% of alumina. More particularly, we try to understand and correlate the structural change due to alumina addition on the variation of elastic and thermodynamic properties. In addition to that we present two methods for the calculation of the elastic properties. For this purpose, we have performed classical molecular dynamics simulations (MD), which provide us a powerful tool to investigate atomic scale behaviour of materials and has been successfully applied to studying behaviour of materials under different thermodynamic conditions and for different systems such as silicate glasses [17–19] and nanocrystalline materials [20,21].

The paper is arranged as follows. In Section 2, we give a detailed description of the simulation method and the interatomic potential used in this work. We describe in details the steps followed to obtain the present results. We give a brief description of the tools used to analyse the structure and compute the different properties. In Section 3, we present the results of this work by trying to correlate the macroscopic properties (thermodynamic and mechanical) to the atomic scale structure of the glass. In Section 4, we give some concluding remarks.

2. Computational details

2.1. Interatomic potential

Molecular dynamics simulations compute the phase space trajectories (Positions r_i and velocities V_i) of a system of particles numerically. In this technique, the time evolution of an ensemble of particles representing the initial structure is tracked by solving the equations of motion of each particle in the considered statistical ensemble. The process is an iterative one in a manner that in each time, atomic positions are known and their velocities are calculated from the forces acting on them. Therefore, we can calculate where the atoms will be after a short period of time known as the timestep (usually in the order of 1 femtoseconds). Then we repeat this procedure for a large number of timesteps. From the phase space, thermodynamic and structural properties can be measured based on ensemble averages as known in statistical mechanics.

The accuracy of MD results depends strongly on the choice of the interatomic function that describes interactions between the system components. In this context, the Born model of solids is the basis for calculating the forces that act on atoms. In this model the particles are treated as charge points interacting via Coulombic interactions with a short-range potential describing interaction between pairs of atoms. The short-range potentials are usually given in terms of parameterized analytical functions, which include both a repulsive term due to electrons overlapping and an attractive one due to the dispersion term or Van der Waals interactions. In the present work, we employed one of the most used potentials, which uses the functional form of Born-Mayer-Huggins (BMH) with the parameterization of Bouhadja et al. [22]. This potential have proven an ability to describe the structural mechanical and dynamics properties of CAS systems [17,18,22]. The functional form of the potential is given by:

$$U_{ij}(r_{ij}) = \frac{q_i q_j}{4\pi\epsilon_0 r_{ij}} + A_{ij} \exp\left(\frac{\sigma_{ij} - r_{ij}}{\rho_{ij}}\right) - C_{ij}/r_{ij}^6 \quad (1)$$

where i and j are atoms (Si , O , Al or Ca), r_{ij} is the distance between atoms i and j , q_i is the effective charge of the atom i , and A_{ij} , σ_{ij} , ρ_{ij} , and C_{ij} are potential parameters given in Table 1. The first term describes the long-range electrostatic interaction between ions, the second one is a short-range Born-Mayer-Huggins exponential term to approximate the overlap repulsion between localized orbitals on nearby atoms, and the last terms represent attraction dispersion terms that takes into accounts for Van der Waals interactions in form of dipole-dipole.

2.2. Glass preparation

The LAMMPS [23] code was used to perform molecular dynamics (MD) simulations and calculate thermodynamic, mechanical and structural properties of calcium aluminosilicate glasses with different alumina concentrations. Seven systems were chosen in this study with

Table 1

Parameters used in Eq. (1) for Bouhadja's potentials, charge of each atom is written as a superscript.

Pairs	$A(eV)$	$\rho(\text{\AA})$	$\sigma(\text{\AA})$	$C(eV\text{\AA}^6)$
$O^{-1.2} - O^{-1.2}$	0.0120	0.2630	3.6430	85.0840
$Si^{2.4} - O^{-1.2}$	0.0070	0.1560	2.5419	46.2930
$Al^{1.8} - O^{-1.2}$	0.0075	0.1640	2.6067	34.5747
$Ca^{1.2} - O^{-1.2}$	0.0077	0.1780	2.9935	42.2556
$Si^{2.4} - Si^{2.4}$	0.0012	0.0460	1.4408	25.1873
$Si^{2.4} - Ca^{1.2}$	0.0027	0.0630	1.8924	22.9907
$Si^{2.4} - Al^{1.8}$	0.0025	0.0570	1.5056	18.8116
$Ca^{1.2} - Ca^{1.2}$	0.0035	0.0800	2.3440	20.9856
$Ca^{1.2} - Al^{1.8}$	0.0032	0.0740	1.9572	17.1710
$Al^{1.8} - Al^{1.8}$	0.0029	0.0680	1.5704	14.0498

Table 2

Details for each composition: molar percentage of Al_2O_3 , SiO_2 , CaO , total number of atoms N , and the glass density ρ from our simulations and available experiment between brackets taken from Takahashi et al. work [24].

Systems	Al_2O_3 % mol	SiO_2 % mol	CaO % mol	N	ρ (g/cm^3)
CS	0	50.0	50.0	4000	2.88 (2.9)
CAS1	5	47.5	47.5	3990	2.85
CAS2	10	45.0	45.0	3990	2.86 (2.86)
CAS3	15	42.5	42.5	4025	2.82
CAS4	20	40.0	40.0	4020	2.82(2.82)
CAS5	25	37.5	37.5	4000	2.83
CAS6	30	35.0	35.0	3998	2.82 (2.81)

different compositions ($CaO - SiO_2$) $_{(1-x)}(Al_2O_3)_x$ where x is the Al_2O_3 molar fraction. Table 2 gives details about the atomic composition of the simulation cells used in the present work, together with the glass densities at room temperature compared with the available experimental densities. A realistic agreement between the present results and those experimentally obtained values is observed.

All systems have around 4000 atoms placed randomly in a cubic simulation box. An integration time step of 1 fs was used. Periodic boundary conditions were applied in all directions to avoid edge effects on the systems. The long-range interactions were evaluated by Ewald summation method, with a cutoff distance of 12.0 Å with a relative error in forces of 10^{-6} . The short-range interaction cutoff distance was chosen to be 8.0 Å. We should mention here that these cutoff values play a critical role in the accuracy of the obtained results and the convergence of the energy, although that they are often omitted in MD works. [17,22]

Firstly, we equilibrated the systems in an NPT ensemble (i.e. isobaric isothermal ensemble) at a high temperature ($T = 4000$ K) and zero pressure for 1 ns. This step is needed to obtain an equilibrated melt as well as to ensure that each system loses its memory of the initial configuration, also this temperature is sufficient to bring our systems to the molten state in the context of the adopted force field. The second step is the linear quenching from 4000 K to room temperature ($T = 300$ K) with a cooling rate of 1 K/ps in the NPT ensemble with zero pressure. Finally, we equilibrated the systems at room temperature in the NPT for 100 ps to relax the system density and energy and used another supplementary 200 ps under NVT ensemble (i.e. canonical ensemble) for statistical averaging. As a matter of fact, cooling rates in molecular dynamics are several orders of magnitude higher than those generally used in experiments due to the intrinsic inability of molecular dynamics (computational power constraints) to use cooling rates lower than 0.01 K/ps. Nevertheless, the values of the cooling rate used in our simulations are often used in many reports and papers [17,25], in addition to that, Li et al. [26] show a dependence of the glass structure on the cooling rate in MD simulations. However, they mention that the short-range order of the glass weakly depend on the cooling rate, while the medium range order is more affected [26].

2.3. Analysis methods and properties calculation

From the obtained phase space, an analysis of the short-range order was made by referring to the pair correlation function, $g_{ij}(r)$, the cumulative coordination function $N_{ij}(r)$ that provides information about the averaged coordination number at a given distance, and bond-angle distribution which presents the angle between three atoms. From these three functions, it is possible to characterise the glass short-range structure since $g_{ij}(r)$ corresponds to the probability of finding a particle i at a distance r away from a particle j . Thus, the first peak of the $g_{ij}(r)$ denotes the average distance between the pair i and j , and the first minimum is used as a cut-off distance to calculate the coordination number of the first neighbour shell. Bond angle distribution is used to estimate the angle between inter and intra tetrahedral units of the

systems.

One way to examine the quenching process of a liquid toward the glass transition is by referring to the concept of the potential energy surface (potential energy landscape PEL) developed by Stillinger [27,28]. The PEL is represented by a $(3N + 1)$ dimensional euclidian space of the potential energy function of N-body, $U(r_1, r_2, \dots, r_N)$, defining a hypersurface with certain topographic features such as saddles, basins, and local minima. Those latter are mechanically stable configurations called inherent structures corresponding to an isolated point in the hypersurface, which is also characterized by a potential energy called inherent structure energy (ISE) [29].

The computation of the ISE is done as follows: at each temperature the phase space trajectory is divided into 10 non-correlated configurations, next we perform an energy minimization through conjugate gradient algorithm (up to a force norm equal to 10^{-6}) of these configurations to bring them to local minima. The ISE at the temperature T is the average of the energy of all these configurations [22].

To calculate elastic properties, the second derivative method was applied. This technique can be used to get the stiffness matrix as well as the compliance matrix. Using a single-point energy calculation the stiffness matrix elements are obtained by:

$$C_{ij} = \frac{1}{V} \left(\frac{\partial^2 U}{\partial \epsilon_i \partial \epsilon_j} \right) \quad (2)$$

By inverting the stiffness matrix, we obtain the compliance matrix:

$$S_{ij} = C_{ij}^{-1} \quad (3)$$

Once the stiffness matrix C_{ij} is found, numerous related mechanical properties of isotropic materials can be derived from their matrix elements such as:

$$B = \frac{1}{9}(C_{11} + C_{22} + C_{33} + 2(C_{12} + C_{13} + C_{23})) \quad (4)$$

$$G = \frac{1}{15}(C_{11} + C_{22} + C_{33} + 3(C_{44} + C_{55} + C_{66}) - C_{12} - C_{13} - C_{23}) \quad (5)$$

$$E = \frac{9BG}{3B + G} \quad (6)$$

The obtained mechanical properties reported in this paper were calculated using two approaches: The first method is by molecular statics through energy minimization at 0 K, and the second one is at a finite temperature in which we used molecular dynamics. At zero temperature, it is easy to calculate these derivatives by deforming the simulation box in one of the six directions and measuring the change in the stress tensor. Calculating elastic constants at finite temperature is more challenging, because it is necessary to run a simulation that performs time averages of differential properties (e.g. stress). One way to do this is to measure the change in average stress tensor in an NVT simulation with temperature control achieved by Langevin thermostat [30] when the cell volume undergoes a finite deformation. In order to balance the systematic and statistical errors in this method, the magnitude of the deformation must be chosen carefully, and care must be taken to fully equilibrate the deformed cell before sampling the stress tensor.

3. Results and discussion

3.1. Glass transition temperature

The quenching process used in our glass preparation was analysed in the basis of the potential energy landscape (PEL). In Fig. 1, we present the evolution of the ISE as a function of temperature for the different considered compositions. The values of the ISE are normalized with respect to that corresponding to 300 K. When the temperature decreases, we observe a rapid decrease in ISE values (Fig. 1), which

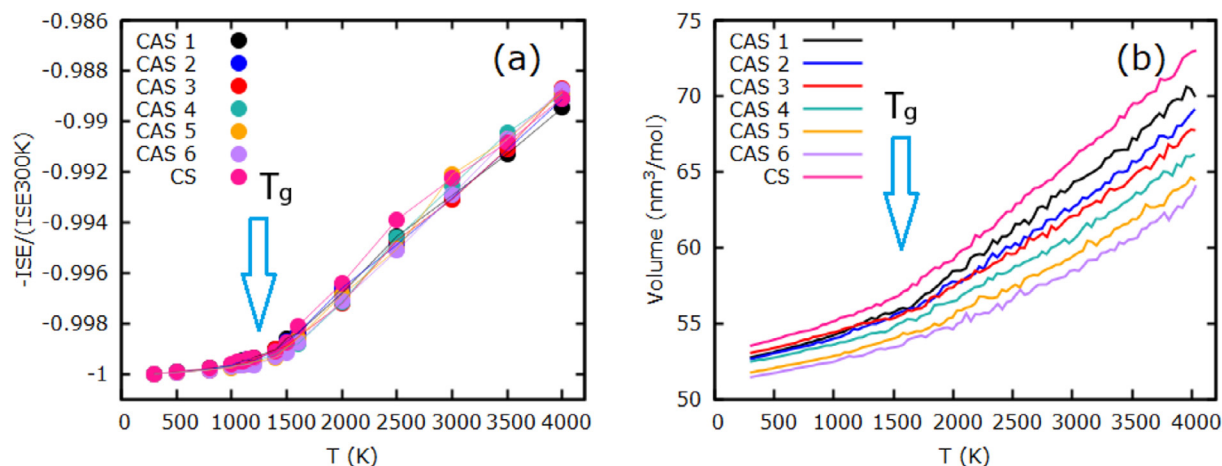


Fig. 1. (a) normalized Inherent Structure Energy (ISE) as a function of the starting temperature and (b) the variation of the molar volume as a function of the temperature for compositions ranging from $x = 0$ to $x = 0.3$. The arrows indicate the glass transition region and lines in (a) are guide for the eyes.

indicates that the systems are unable to cross highest energy barriers resulting in a gradual trapping in deep minima. At high temperatures, atoms have high kinetic energies, which gives them a great deal of freedom in their ability to rearrange. In contrast, as the temperature decreases the atoms mobility start to decrease rapidly, which results in a slowing down of the system dynamics [31]. Around the glass transition temperature T_g , a change of the slope is observed, indicating that the system falls out of equilibrium and the system is found in a state called the frozen state which has a structure quiet similar to its parent the supercooled liquid just above T_g [32]. This means that the relaxation time of the system starts to exceed the observation time. The glass transition values are determined from the slop break between low and high temperature branches of the ISE curves. The resulting glass transition values were also found from the slop break between low and high temperature branches of the $V(T)$ curves, where V denotes the molar volume of the system.

Table 3 presents T_g values obtained using the ISE method as a function of the $\text{CaO}/\text{Al}_2\text{O}_3$ ratio together with those obtained using the volume variation with temperature method and eventually available experimental results. We obtained a systematic increase in T_g values with increasing alumina content for both methods. The slight increase in T_g as the Al_2O_3 content increases indicates that aluminium in tetrahedral coordination [33] plays a role similar to silicon, i.e., a network forming role in a three-dimensional network. This is also due to the transformation of Ca atoms from network modifiers to charge compensators.

Moreover, as shown in Fig. 2, the values obtained from the ISE are in a good agreement with the experimental values. We mention that that for CAS6 the experimental T_g value is obtained for a closer composition. Table 3 and Fig. 2 show that T_g values found via the volume-

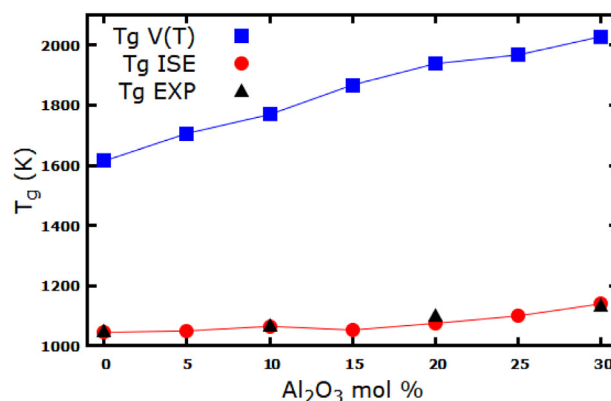


Fig. 2. The glass transition temperature T_g as a function of alumina content compared to experimental values. The blue dotted line presents T_g values obtained using the volume variation with the temperature and the red dotted line stands for T_g values obtained using the ISE method. Experimental values are taken from reference (24). Lines are guide for the eyes. (For interpretation of the references to colour in this figure legend, the reader is referred to the web version of this article.)

temperature curve are larger than both experimental and ISE values; this can be attributed to the high quenching rates used in molecular dynamics that makes the system trapped in high energy local minima, whereas during the ISE calculation the system is brought out of the trap by minimizing its potential energy.

3.2. Structural properties

The local structure around silicon, aluminium and calcium atoms are well captured by the partial radial distribution functions (PDF). The distribution functions for these three pairs are presented in Fig. 3(a, c) and 4(a). The integration of the first peak of the PDF gives information about the coordination number defined as $n_{ij}(r) = \frac{N}{V} \int_0^r 4\pi r'^2 g_{ij}(r') dr'$ where N stand for the number of atoms, V the volume and r_c is the cutoff value which was chosen to be 2.1, 2.2 and 3.1 for $\text{Si}-\text{O}$, $\text{Al}-\text{O}$, and $\text{Ca}-\text{O}$ respectively. These cutoff values are taken to be the same for all compositions. For $\text{Si}-\text{O}$, $\text{Al}-\text{O}$ and $\text{Ca}-\text{O}$ PDFs, the first peak position which is the average distance between each pair is unaffected by adding the alumina to the system. The $\text{Si}-\text{O}$ partial correlation function shows a sharp first peak while it vanishes to zero for distances between 1.8 and 2.5 Å, showing the strong covalent nature of the $\text{Si}-\text{O}$ bond. Compared to $\text{Si}-\text{O}$ bond, the $\text{Al}-\text{O}$ bond presents a similar behaviour, but with a less intense and wider first peak and with a non-

Table 3

Values of the glass transition temperature T_g as a function of composition and the ratio $\text{CaO}/\text{Al}_2\text{O}_3$ compared to experimental values. Values of column 3 are obtained using the ISE method and those in column 4 are obtained using the volume variation with temperature. Error values are estimated from the uncertainty of the slope of the linear fitting.

Systems	R = $\text{CaO}/\text{Al}_2\text{O}_3$	$T_g \pm 20 \text{ K(ISE)}$	$T_g \pm 30 \text{ K(V(T))}$	$T_g \text{ EXP (K)}$
CAS1	9.5	1050	1706	–
CAS2	4.5	1065	1769	1069 [24]
CAS3	2.83	1053	1867	–
CAS4	2	1075	1938	1099 [24]
CAS5	1.5	1100	1967	–
CAS6	1.16	1140	2028	1132 [24]
CS	–	1045	1615	1050 [24]

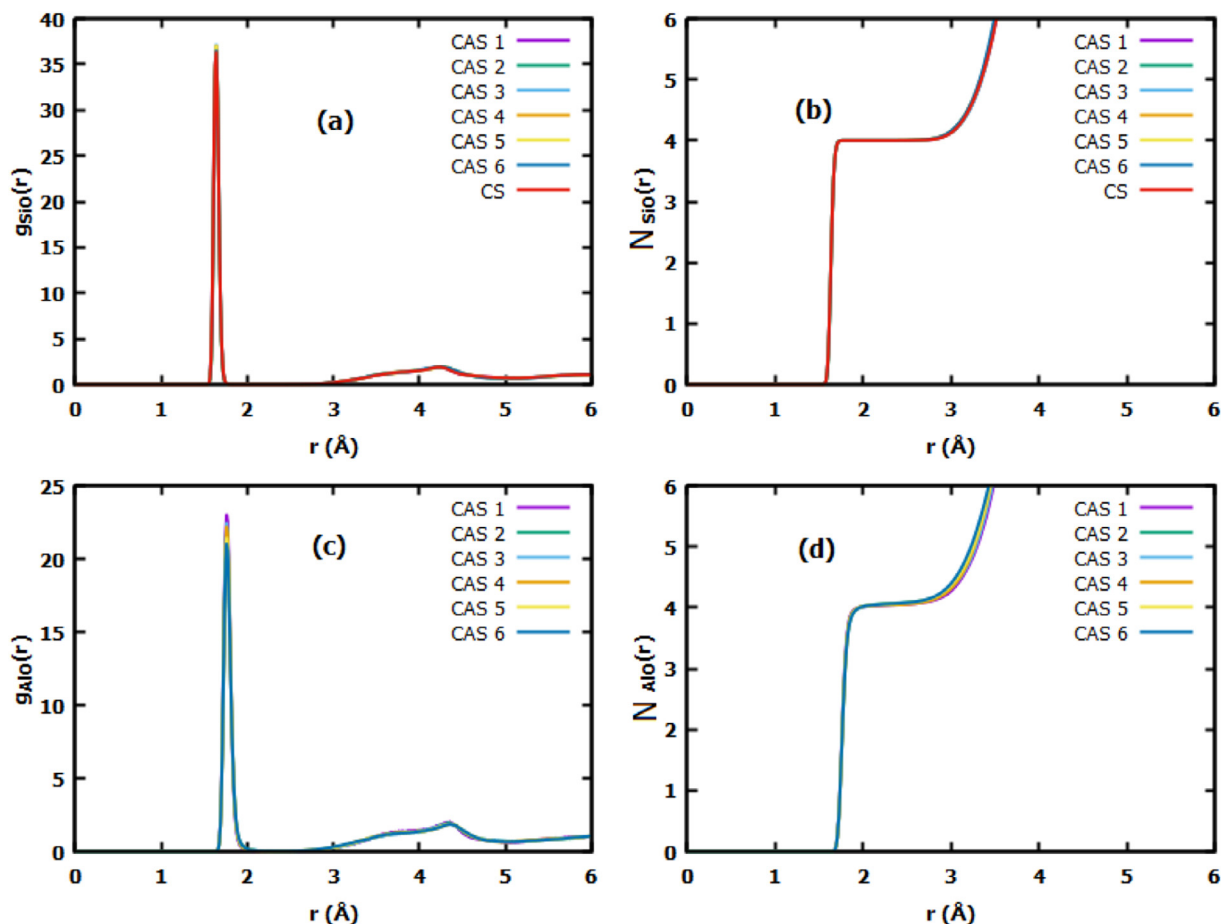


Fig. 3. Pair correlation functions and cumulative coordination numbers of (a, b) Si–O pair and of (c, d) Al–O pair for different alumina contents at 300 K.

zero first minimum, indicating that Al–O bonds are more flexible than the Si–O bonds (e.g. possibility of presence of larger bonds). In addition, the first peak of the Al–O correlation function shows a maximum at a distance around 1.75 Å which is in a good agreement with ab initio and experimental results [14,18]. The higher values of the Al–O bond length is explained by the existence of five and/or six-fold coordinated Al. Indeed, the Al–O bond length in five-fold coordinated Al (1.83 Å) [34] and in six-fold coordinated Al (1.91 Å) [35] are longer than that corresponding to four-fold coordinated Al (1.81 Å) [36]. The shift in Al–O PDF was not obtained in the present study; this is due to the dominance of four-fold coordinated Al atoms with a small fraction of five-fold Al atoms. This result indicates that no dramatic change in the Al coordination number occurs as the composition varies. Furthermore, neither Si–O nor Al–O bond lengths are affected by the relative composition, since there is no shift in the first peak with increasing Al_2O_3 . [2]

The curve of Ca–O PDF has a first minimum amplitude ranging from 0.3 to 0.6 depending on alumina concentration (Fig. 4). This can be explained by a possible breaking of Ca–O bonds. Knowing that an exact determination of the local environment of the modifier cation is challenging due to the proximity of the partly overlapping O–O pairs, as mentioned by Cormier et al. [37], the structure of the glasses corresponds to a frozen structure of the liquid state. In a recent study by Li et al. [26], in sodium silicate glasses, it has been shown that the structural differences due to different quenching rates do not affect the silicate polymerization state.

The evolution of the first peak of the function $g_{o-o}(r)$, presented in Fig. 4 (c), gives information on intra- and inter-tetrahedra O–O correlations. Unlike the other three pair correlation functions, the position of the first peak shifts toward larger r values with the increase of the

alumina concentration. It varies from 2.64 Å for CS, close to the O–O distance in SiO_4 tetrahedra, to 2.74 Å which is the characteristic distance of the O–O bond in AlO_4 tetrahedra. This evolution suggests the occurrence of a progressive replacement of SiO_4 tetrahedra by AlO_4 tetrahedra when the alumina content increases. The first peak becomes less intense and wider; however, its intensity shows a minimum for 30% of alumina. This behaviour is also observed in other studies that focused on the effect of adding silica to calcium aluminosilicate glasses [22,37].

Our analysis of the cumulative coordination numbers presented in Fig. 3(b) and (d), and summarized in Table 4, shows that for all compositions Si–O and Al–O pairs have an average coordination number equal to 4, which means four oxygens in their first coordination shells. The Ca–O pair presented in Fig. 4 (b) and Table 4, has a coordination number around 6 and a pair distance of 2.35 Å for all different glass samples. These values are in a good agreement with Ca in octahedral sites ($d_{Ca-O} = 2.4$ Å) as mentioned for calcium silicate glasses [38] and calcium aluminosilicate glasses [22]. The shape of these octahedrons is disordered, which implies that the structure do not present a well-defined symmetry [39,40] as shown in Fig. 5b and d.

The partial radial distribution functions (PDFs) for the different system components displayed in Fig. 6 (a, c, e, g) can help in understanding how polyhedral clusters are connected. From these distributions functions we can notice a first peak at 3.0 Å, 3.15 Å, 3.11 Å and 3.25 Å for Si–Ca, Al–Ca, Al–Al, and Si–Si, respectively. In addition, we observe the presence of a second peak for Al–Ca and Si–Ca PDFs at 3.5 Å, and 3.7, respectively. A deeper investigation of the structure allowed us to suggest that the first peak of the Al–Ca and Si–Ca PDFs is attributed to BOs while the second peak is mainly due to NBOs, thus silicon atoms are mainly surrounded by NBOs and aluminium atoms are mainly surrounded by BOs. As the alumina content increases

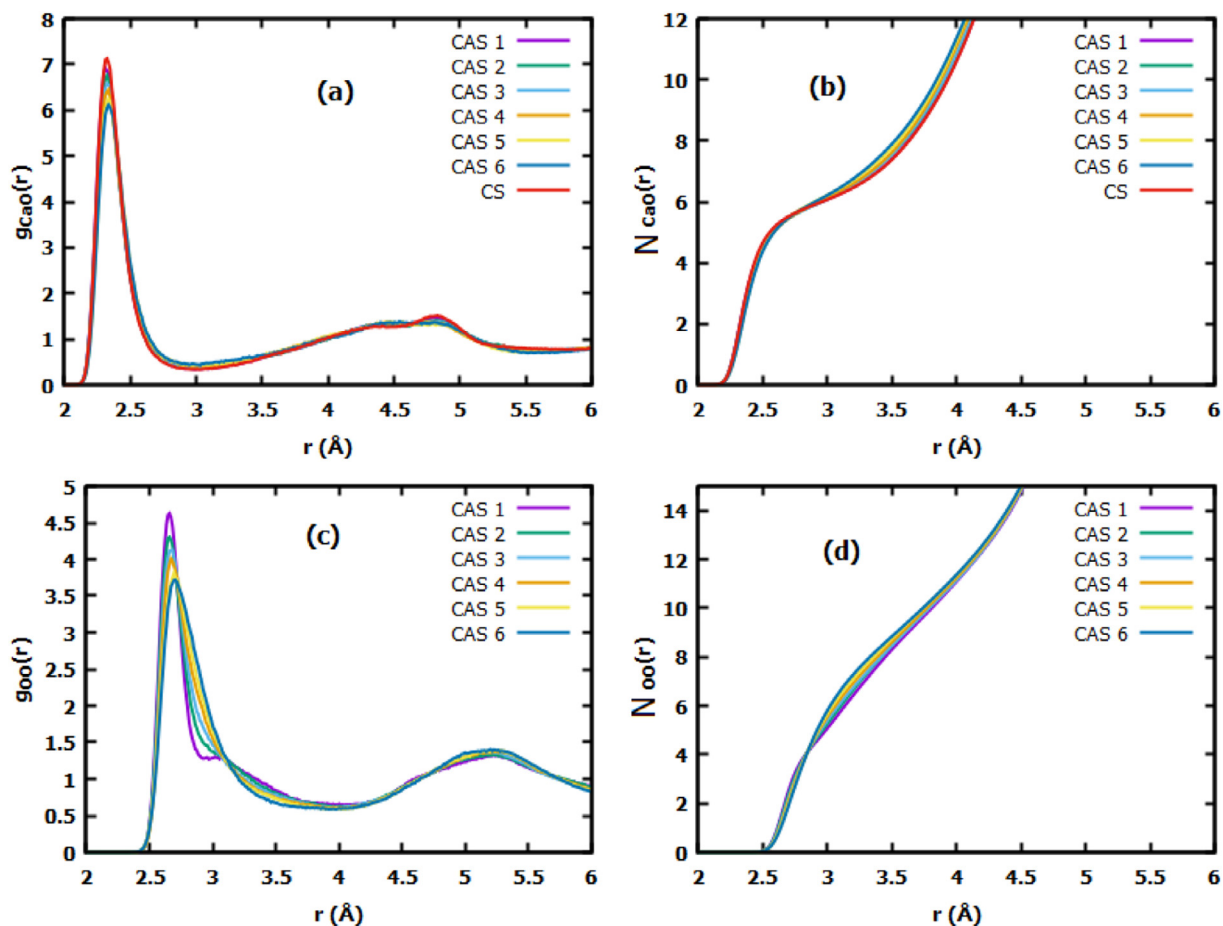


Fig. 4. Pair correlation functions and cumulative coordination numbers of (a, b) Ca–O pair and of (c, d) O–O pair for different alumina contents at 300 K.

Table 4

Summary of the first peak position and coordination number of the different atoms surrounded by oxygen atoms obtained by MD simulation at 300 K and averaged over 200 configurations. The average distances $r_{i-j} \pm 0.02 \text{ \AA}$.

Sample	Si–O		Al–O		Ca–O		O–O	
	$r \text{ (\AA)}$	CN	$r \text{ (\AA)}$	CN	$r \text{ (\AA)}$	CN	$r \text{ (\AA)}$	CN
CAS1	1.638	4.00	1.755	4.02	2.31	6.07	2.65	5.07
CAS2	1.638	4.00	1.757	4.031	2.32	6.10	2.65	5.26
CAS3	1.639	4.00	1.756	4.021	2.32	6.09	2.68	5.39
CAS4	1.638	4.00	1.758	4.028	2.33	6.14	2.68	5.54
CAS5	1.637	4.00	1.757	4.031	2.33	6.20	2.69	5.67
CAS6	1.638	4.00	1.758	4.025	2.33	6.20	2.74	5.81
CS	1.636	4.00	–	–	2.32	6.06	2.64	4.91

(decreasing of calcium oxide content) the number of BOs around aluminium atoms start to increase which is shown by the augmentation of the intensity of the first peak of the Al–Ca PDFs. From the PDFs of Si–Si and Al–Al we can estimate the distance between two SiO_4 tetrahedra and that separating two AlO_4^- tetrahedra, respectively. Indeed, the first peaks observed at 3.25 \AA for Si–Si bond and at 3.11 \AA for Al–Al bond correspond to the distances between centres of SiO_4 and AlO_4^- tetrahedra, respectively.

The behaviour of the cumulative coordination numbers of the Si–Ca, Al–Ca, Al–Al, Si–Si presented in Fig. 6 (b, d, f, h) agrees with our observation that silicon atoms are surrounded mainly by BOs and aluminium atoms are initially surrounded by NBOs. Moreover, the increase of the alumina content that came also with the decrease of CaO content leads to an increase of the amount of BOs with a decrease of Si–O–Ca and Al–O–Ca linkages showing a high dependence on

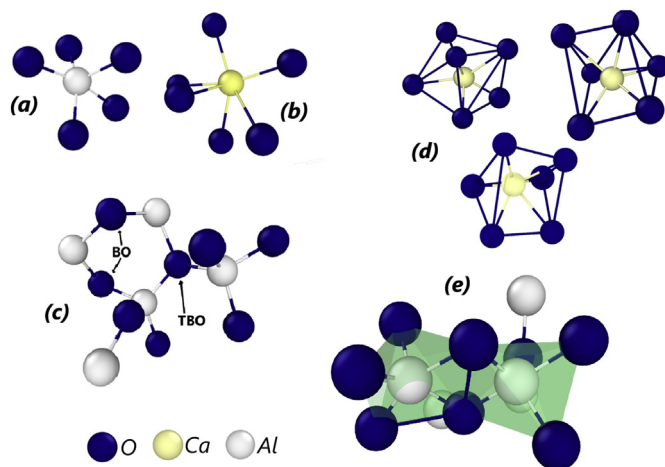


Fig. 5. Snapshots showing (a) AlO_5 , (b) CaO_6 , (c) bridging oxygens and oxygen tricluster, (d) example of disordered calcium octahedra and (e) edge-sharing tetrahedra present in the glass structure obtained from our simulation at 300 K. grey atoms are Aluminium, blue atoms represent Oxygen and yellow atoms are Calcium. (For interpretation of the references to colour in this figure legend, the reader is referred to the web version of this article.)

composition changes.

Otherwise, the calculation of bond angle distributions gives additional information regarding the short- and medium-range orders around Si and Al atoms through the angles between different bonds in each tetrahedron and the angles between tetrahedra themselves. Thus, as shown in Fig. 7(a), SiO_4 tetrahedra in these glasses are built-up by

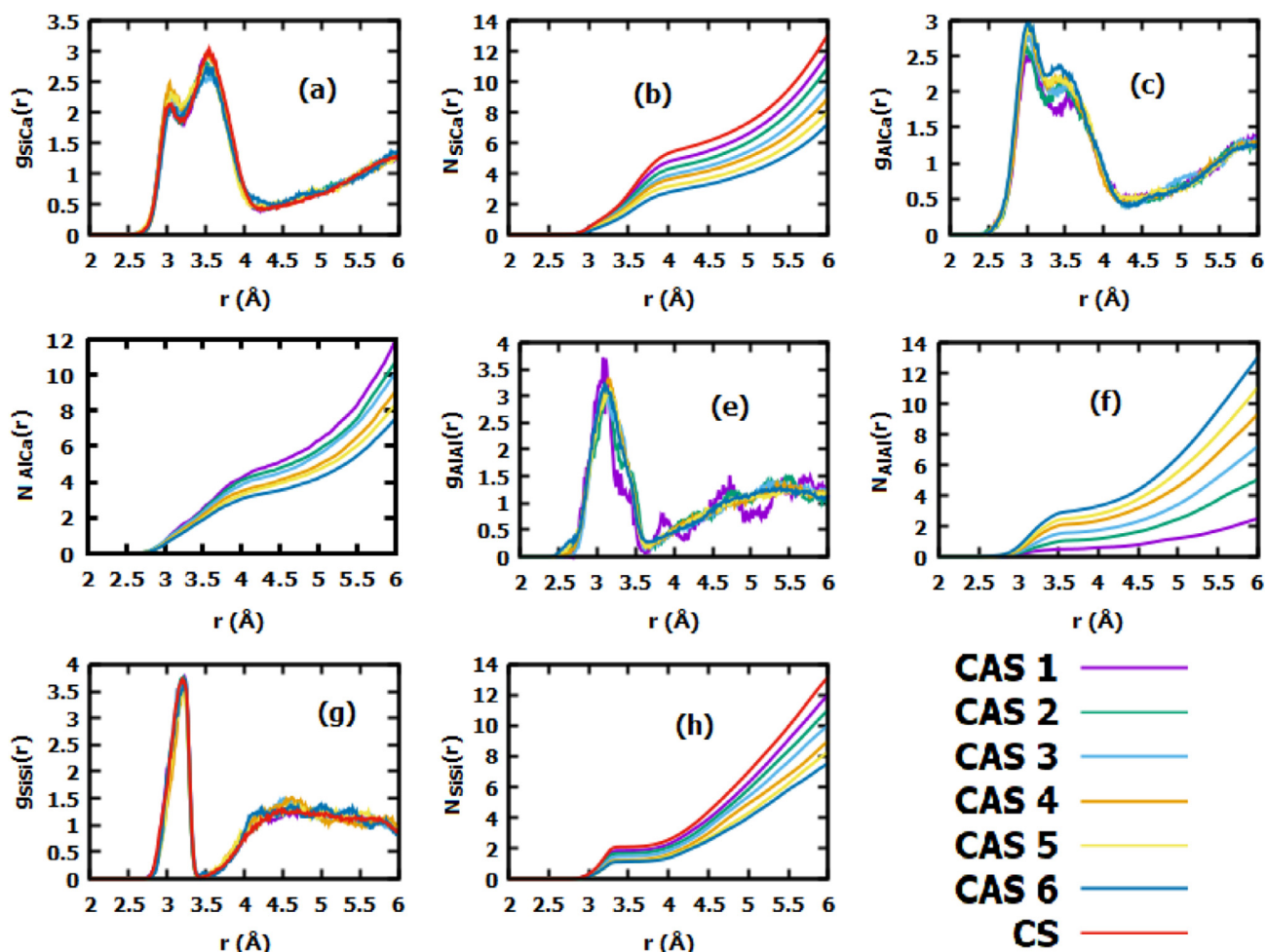


Fig. 6. Pair correlation functions and cumulative coordination numbers of (a), (b) Si–Ca, (c), (d) Al–Ca, (e), (f) Al–Al, and (g), (h) Si–Si, for different glass compositions obtained at 300 K.

O–Si–O bond angles centred at 108.2° , which is very close to the value in a perfect tetrahedral geometry (109.4°). Generally, the nearest neighbour environments around Si did not show any difference for all considered compositions. From another side, Fig. 7(b) shows that the O–Al–O bond angle distribution is broader than that of O–Si–O and is centred around 107.2° with a shift to lower values as the alumina content increases. This confirms the distorted tetrahedral nature of the AlO_4^- tetrahedra, and the broadening of the distribution indicates the presence of some irregular shape of AlO_4^- polyhedra.

The Si–O–Si and Al–O–Al bond angle distributions presented in Fig. 7 (c) and 7 (d) provide supplementary information on the linkage between SiO_4-SiO_4 and $AlO_n^{(n-3)-}-AlO_n^{(n-3)-}$, ($n = 4$ or 5) polyhedra. We observe that Si–O–Si bond angle starts from 140.25° for the calcium silicate system and increases with increasing alumina content reaching a value of 147.2° . The Si–O–Al bond angle distributions shown in Fig. 7 (e) represent the angle of linkage between a SiO_4 tetrahedron and an AlO_4^- tetrahedron. It is observed that the value of the angles is centred at 135° and it decreases to 130° as the alumina content increases. The Al–O–Al distribution shows a main peak around 120° with a small peak around 160° in CAS1 with 5 mol% alumina, while it is centred around 125° for the other compositions. From this, we can see the violation of the aluminium avoidance principle through the existence of Al–O–Al linkage in our systems [41], as the bond angle distributions are calculated using the atoms in the first coordination shell.

In this context Allu et al. [42] derived a parameter called the Aluminium Avoidance Parameter (AAP) to predict when there are enough

O–Si bonds to satisfy the aluminium avoidance principle, this parameter is given by:

$$AAP = \frac{4[Al_2O_3]}{2[SiO_2] - [RO] + [Al_2O_3]} \quad (7)$$

where RO stands for CaO in the present case. Allu et al. [42] stated that when $AAP \leq 1$, there is enough O–Si bonds to satisfy the Aluminium avoidance principle. Thus Si–O–Al bond are more favourable than Al–O–Al bonds. Otherwise, there is less O–Si bonds in the glass network which results in the violation of the aluminium avoidance principle. In our glass samples the calculated AAP values are 0.38, 0.73, 1.04, 1.33, 1.6 and 1.85 for CAS1, CAS2, CAS3, CAS4, CAS5 and CAS6 respectively. As a result, in the glasses CAS3, CAS4, CAS5 and CAS6 there is less O–Si bonds to satisfy the aluminium avoidance principle. In these cases, the remaining Al_2O_3 breaks the rule and forms Al–O–Al linkages of $AlO_n^{(n-3)-}$ polyhedra. This will result in a separation of the glass network into a region made by SiO_4 tetrahedra and another one made by SiO_4 tetrahedra and $AlO_n^{(n-3)-}$ polyhedra separated by a non-network cations channel. To get more insights, we did calculate the percentage of the Si–O–Si, Al–O–Al, and Si–O–Al linkages found in our glasses CAS1-CAS6, as illustrated in Fig. 8 from the plot we see that Al–O–Al increases linearly with the AAP as expected. Moreover, Si–O–Al linkage increase in a nonmonotonic way with AAP up to 20% of alumina and start decreasing, while the Si–O–Si decreases also in a nonlinear way. However, from the AAP it is expected that there is no Al–O–Al linkage for values lower than 1, in our study we did find Al–O–Al linkage even at AAP values lower

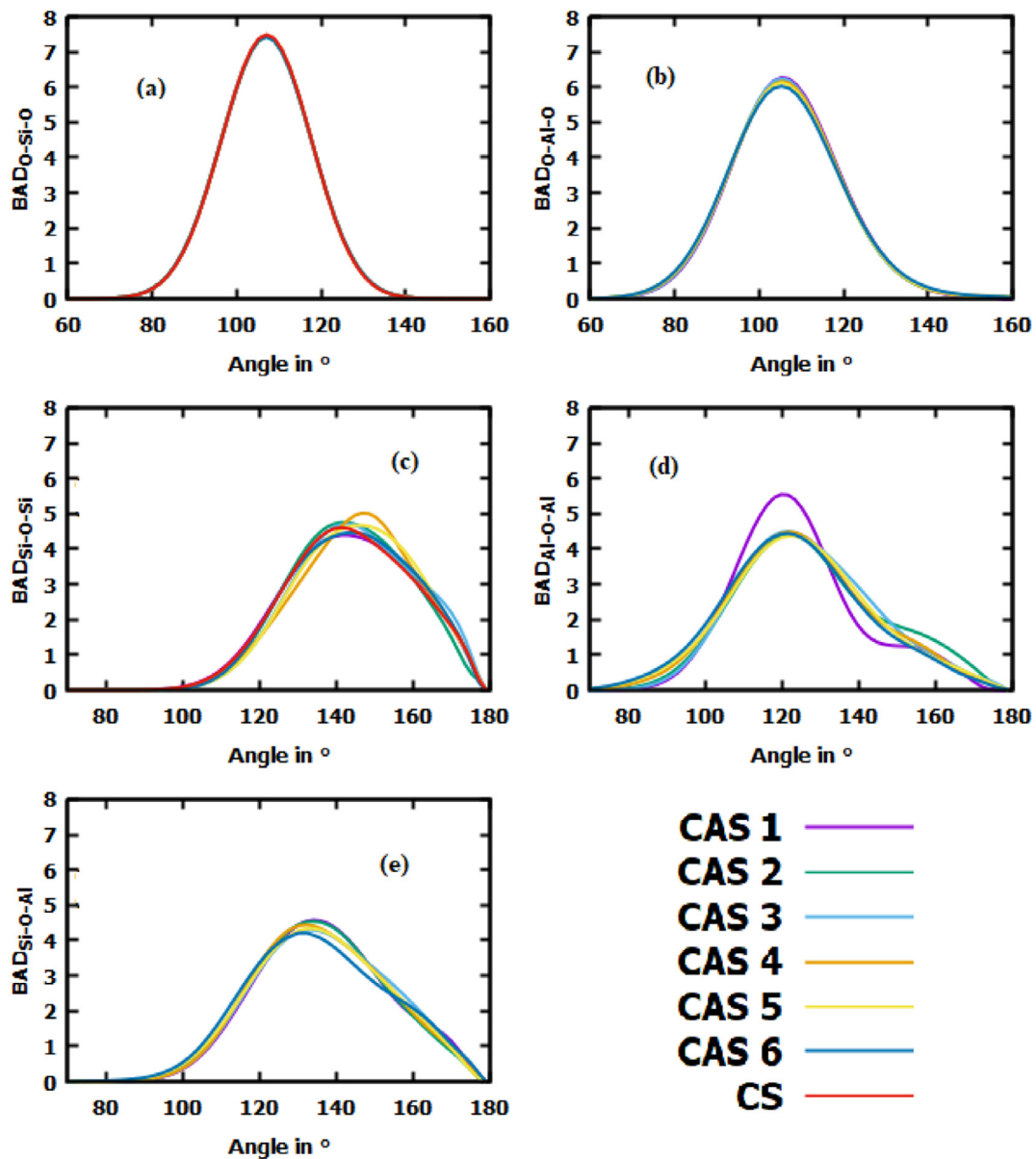


Fig. 7. Bond angle distribution for (a) O-Si-O, (b) O-Al-O, (c) Si-O-Si, (d) Al-O-Al, and (e) Si-O-Al for different Al compositions at 300 K.

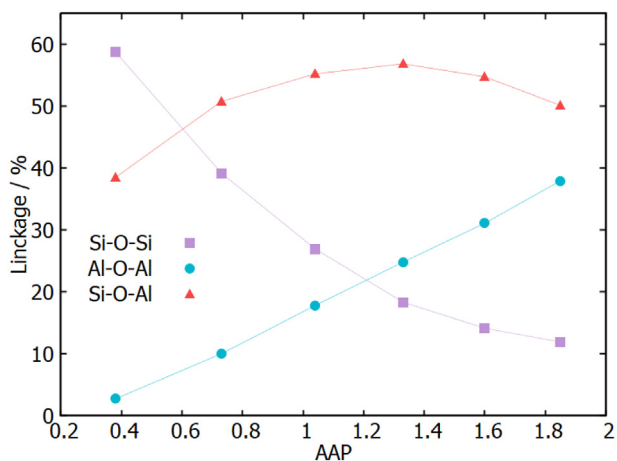


Fig. 8. Si-O-Si, Al-O-Al, and Si-O-Al as a function of the aluminium avoidance parameter in our glass systems at 300 K.

Table 5

Change of oxygen speciation with glass composition computed from MD simulations and compared to the model of Eq. 8.

System		FO (%)	BO (%)	NBO (%)	TBO (%)
CAS1	MD	1.21	46.91	51.8	0.08
	Model	-	46.03	53.97	-
CAS2	MD	0.92	56.47	42.1	0.5
	Model	-	57.56	42.44	-
CAS3	MD	0.21	65.6	33.45	0.74
	Model	-	68.12	31.88	-
CAS4	MD	0.20	73.14	24.05	2.61
	Model	-	77.78	22.22	-
CAS5	MD	0.1	79.1	16.5	4.3
	Model	-	86.67	13.33	-
CAS6	MD	0.04	82.1	11.26	6.6
	Model	-	94.92	5.08	-
CS	MD	1.2	34.3	64.5	-
	Model	-	33.33	66.67	-

than 1 but with a small fraction (<10%).

3.3. Oxygen species and polyhedral connection

The oxygen species are of great interest due to their relation to the structural change and macroscopic glass properties. Table 5 shows the oxygen species categorized into four oxygen types: The bridging oxygens connected to two network formers, non-bridging oxygens connected to only one network former, oxygen triclusters connected to three network formers, and free oxygens connected only to network modifiers. Fig. 5(c) shows examples of bridging oxygens and oxygen tricluster obtained during the present simulations. If we consider that the glass network was made only of tetrahedra inter-connected by twofold coordinated oxygen atoms [43], then the predictable number of NBO atoms in the systems can be assessed from a simple relation between N_{Ca} and N_{Al} , given by:

$$N_{NBO} = 2N_{Ca} - N_{Al} \quad (8)$$

Or directly from the composition expressed by the mole fractions [44] as follow:

$$f(NBO) = \frac{2([CaO] - [Al_2O_3])}{[CaO] + 2[SiO_2] + 3[Al_2O_3]} \quad (9)$$

Since both models give almost the same result, we present here only values obtained from Eq. (8). As shown in Fig. 9(a) and Table 5, the computed fractions of the different species obtained by MD simulations are in good agreement with this model for all considered compositions.

As shown in Table 5, there is an increase of the number of BOs and a decrease of that of NBOs with increasing Al_2O_3 content (the ratio $R = CaO/Al_2O_3$ decreases). This effect has been also observed for other compositions [9] not considered in the present work. Thus, with increasing alumina content, one theoretically expects an increase of the network connectivity accompanied by a decrease in the population of the NBO and free oxygens. The presence of these FOs could be just an artefact due to the high cooling rate used herein. Moreover, the oxygen triclusters should increase with increasing alumina content, which supports the mechanism of neutralization of the extra negative charge around $[AlO_4]^-$ when there is not enough Ca^{+2} for charge compensation. Moreover, there is an increase of the amount of AlO_5 clusters

which act as charge compensator as suggested in many works, not only in Calcium aluminosilicate [37,45] but also in sodium aluminosilicate glasses [2,46].

One way to determine the connectivity in glasses and melts is the degree of polymerization, which is a factor directly linked to the composition of silicate glasses and melts. The degree of polymerization can be determined by the coefficient BO/Si , which is the ratio between the number of Bridging oxygens and the number of silicon (Si) atoms in the glass [47]. If the glass contains other network forming cations, the coefficient is calculated as the ratio between the number of Bridging oxygens and the sum of the numbers of network-forming cations (T) (in this study $T = Si + Al$) [48]. The degree of depolymerization of a silicon–aluminium–oxygen network is frequently represented by another structural factor, which is designated as NBO/T . This parameter is defined as the ratio between the number of non-bridging oxygen atoms and the total number of network former atoms in the glass. Fig. 9 (a, b) presents the degree of polymerization and depolymerization as a function of alumina content, obtained by both molecular dynamics simulations and the model presented above (Eq. 8). From this figure we can see that the connectivity of the glass network increases with increasing alumina content, this can be attributed to the synergy between Al atoms in forms of AlO_4 tetrahedra and Si atoms in forms of SiO_4 that contribute to the formation of the network. Furthermore, the decrease of calcium oxide content leads to a decrease in the ratio CaO/Al_2O_3 and then to the transformation of the calcium cations from network modifiers to charge balancing cations.

It is well known that the connection between SiO_4 tetrahedra occurs through corner-sharing oxygens which has been found in the present simulations as shown in Fig. 10 (a), where all SiO_4 tetrahedra are connected via a corner-sharing mode. However, for AlO_4^- tetrahedra, as the alumina content increases the fraction of corner-shared tetrahedra starts decreasing with a small increase in the number of edge-shared tetrahedra (see Fig. 5(e)). This effect takes place starting from 15 mol% of alumina (CAS3) and keeps increasing as shown in Fig. 10(b).

This effect is also accompanied by an important increase of TBO as presented in Table 4, which suggests that the presence of TBO in the system can help creating other modes of linkage between tetrahedra. Fig. 10 (c) shows an increase of the average coordination number of

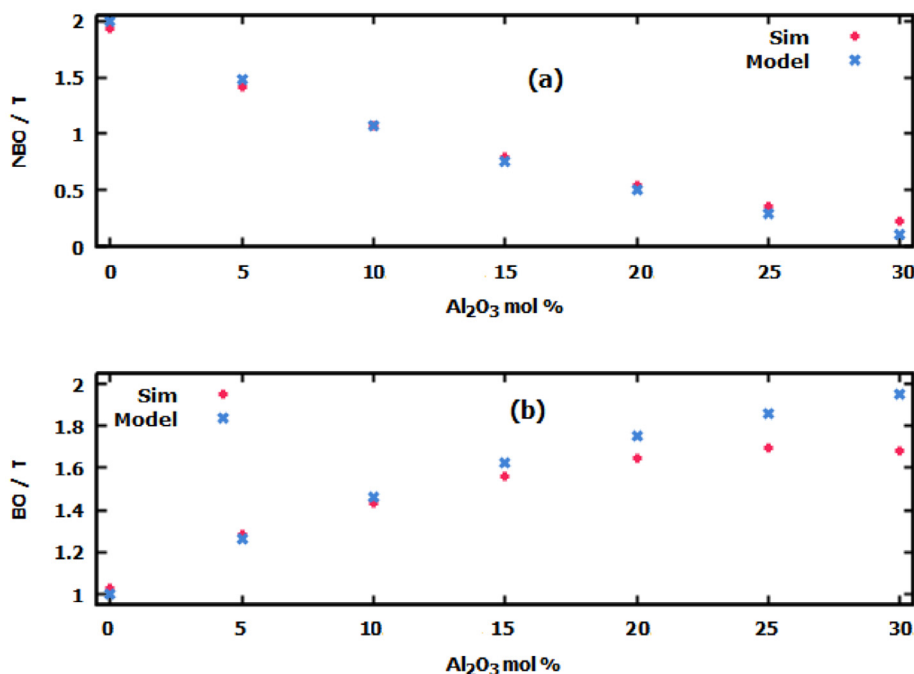


Fig. 9. NBO/T and BO/T as a function of alumina content obtained from MD simulations at 300 K and from the model of Eq. 8.

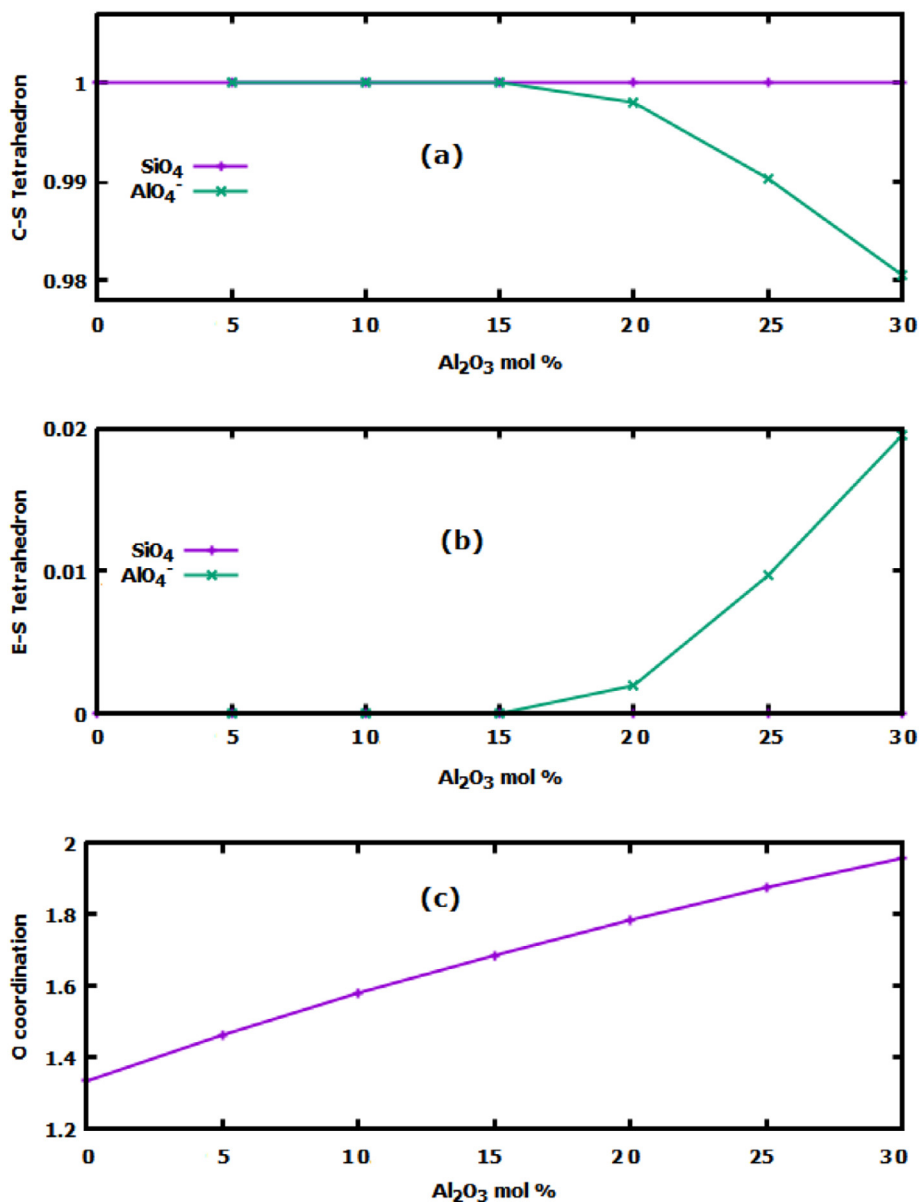


Fig. 10. (a) and (b) are the normalized Edge-sharing and Corner-sharing silicon and aluminium tetrahedron as a function of the composition and (c) is the averaged oxygen coordination number with respect to other elements (Si, and Al) as a function of the composition obtained by MD simulations at 300 K.

oxygen atoms as the alumina content increases indicating the presence of larger amount of silicon and aluminium in the environment of oxygens. This confirms our previous statement that increasing alumina content leads to an increase of BO and TBO.

3.4. Rings statistics

RINGS code was used to calculate the ring size distribution [49]. As a matter of fact, there are several definitions of rings and multiple algorithms to calculate the rings and give their distribution. In this study, we calculated the rings following Guttman definition, in which a ring is defined as the shortest closed paths within the calcium aluminosilicate network. The ring size is defined as the number of Si or Al atoms that belong to a given ring.

Fig. 11 illustrates the ring size distributions. The overall behavior is in agreement with previous simulation studies [9]. Starting from the calcium silicate glass (CS), we observe that the addition of Al₂O₃ enhance the formation of rings with different sizes. However, as the amount of Al₂O₃ keeps increasing, we observe that rings with sizes

between 4 and 7 increased. Those rings are nearly absent in the CS glass. This can be understood from the fact that, at low amount of Al₂O₃, the structure is mainly made by Q² structural units (see Fig. S1) in the form of SiO₄ chains and large rings. Upon adding Al₂O₃, Al atoms tend to form AlO₄⁻ units that are charge compensated by Ca cations (see Fig. 3 d and Table 4). Replacing Al by Si atoms results in an increase of the five-membered rings. The addition of each Al atom thereby effectively consumes one NBO, as Ca turns from a network-modifying to a charge compensating role. This induces an increase in the overall connectivity of the glass (see Table 5 and Fig. 9), which results in the formation of small rings.

3.5. Mechanical properties

In this section, we focus on the composition and temperature dependence of the calculated elastic properties. Elastic moduli are calculated using the two methods described in Section 2, one is via molecular statics using energy minimization and the other by performing molecular dynamics at a finite temperature. Figs. 12 (a – c) present the

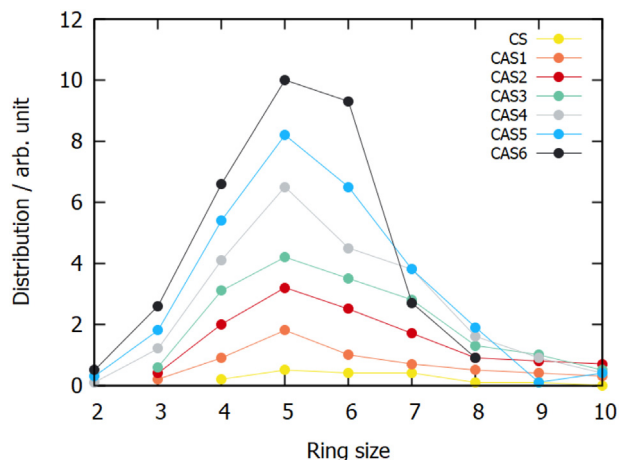


Fig. 11. Computed ring size distribution for different compositions in this study. The distribution is plotted as a function of the number of Si and/or Al atoms in the rings at 300 K. Lines are guide for the eye.

effect of alumina content on the elastic moduli calculated by both methods for the calcium aluminosilicate glasses.

As presented in Fig. 12, there is a difference between elastic constants calculated at 0 K and those computed at 300 K. Elastic moduli found at 300 K are generally lower than those obtained at 0 K, which is mainly attributed to thermal fluctuations created by vibrational motion of atoms. Furthermore, due to thermal expansion the molar volume of the sample at 0 K is lower than that obtained at 300 K, which increases the atomic packing density by squeezing out extra volume as can be indicated by the difference in the density (not shown here), thus leading to higher elastic properties at 0 K. In comparison with available

experimental data at room temperature [50] of a relatively closer compositions, we can notice that the elastic properties calculated at finite temperature are much closer to experimental values which indeed puts a light on the importance of taking into account thermal vibration of atoms when calculating mechanical properties. It is also needed to stress out that the calculation of the elastic properties can be affected by the size of the systems, the quenching rate and/or the transferability of the interatomic potential used here to different compositions in the CaO-Al₂O₃-SiO₂ ternary diagram.

Fig. 12 (d) illustrates the variation of elastic moduli as a function of the degree of depolymerization (*NBO/T*). Therefore, we can see that the Young's modulus (*E*), the bulk modulus (*K*), and the shear modulus (*G*) increase with increasing alumina content. Experimentally, such trends are also observed in Young's, bulk, and shear moduli [51]. The variation of elastic properties as a function of the network connectivity shows also an increase of the elastic moduli with the increase of the degree of polymerization. The Young's modulus increases from 96.97 GPa to 106.85 GPa, the bulk modulus increases from 77.10 to 85.75 GPa and the shear modulus keeps fluctuating between 37.27 GPa and 40.94 GPa with increasing alumina content. Therefore, as alumina content increases the glasses become more packed and rigid showing that all elastic moduli increase. The increase in Al₂O₃ content enhances the atomic packing density and total dissociation energy of the glass because of the large dissociation energy of Al₂O₃ per unit volume compared to that of SiO₂ [8]. As a result, the glass with the highest Al₂O₃ content (*x* = 30) shows the highest values of the elastic modulus. These effects has been also observed in other systems, such as Na₂O-SiO₂-Al₂O₃, R₂O₃-SiO₂-Al₂O₃, MO-SiO₂-Al₂O₃ or Al₂O₃-SiO₂ glasses, and crack-resistant silicate or borosilicate glasses [2,52-61].

For the composition having 15% of alumina, we observed structural transition which manifests itself through a change in the elastic moduli.

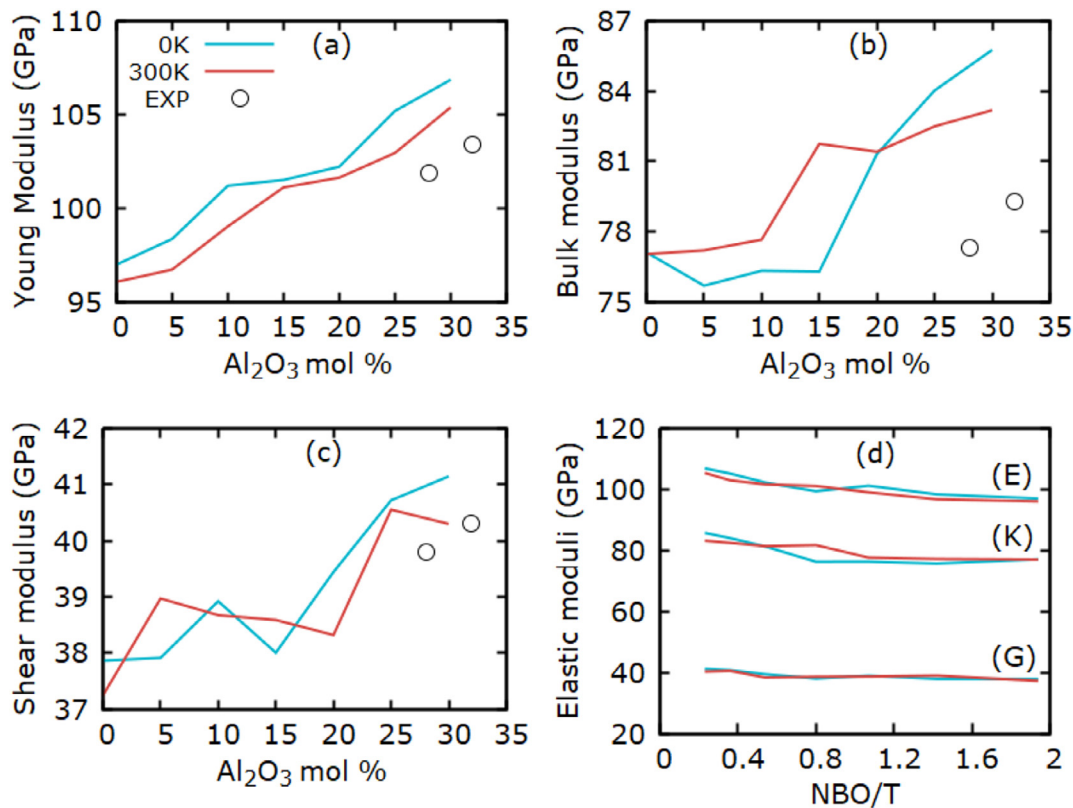


Fig. 12. a), b), and c) present the effect of alumina content on elastic moduli calculated by both methods, as described above, in the calcium aluminosilicate glasses with experimental values found in Pönitzsch et al. work [50], of a relatively closer composition, d) illustrates the variation of elastic moduli as a function of the degree of depolymerization.

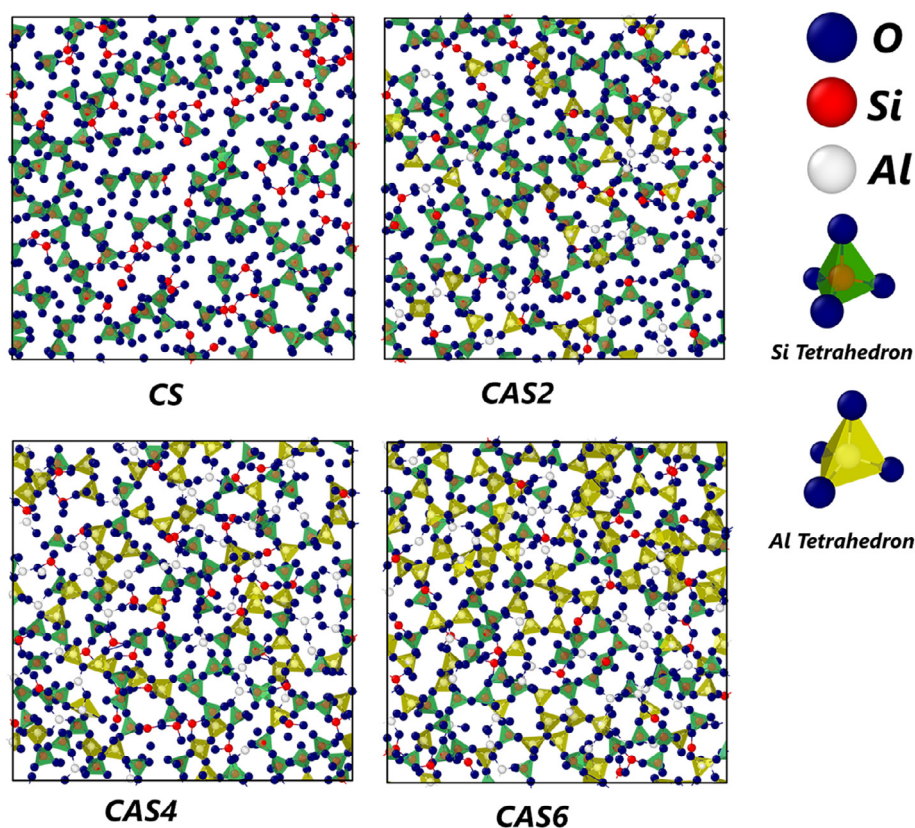


Fig. 13. Snapshots showing the structural change due to the addition of alumina into calcium silicate network, calcium atoms are not visualized and the green and yellow polyhedrons stand for silicon and aluminium tetrahedra. Top left shows calcium silicate, Top right presents CAS2, bottom left is for CAS4, and bottom right for CAS6. Blue atoms represent Oxygen, red atoms are Silicon, and grey atoms stand for Aluminium. The snapshots show clearly that the network becomes more and more packed and connected as the alumina content increases, which enhances the rigidity of the network and also results in an increase in T_g and mechanical properties. (For interpretation of the references to colour in this figure legend, the reader is referred to the web version of this article.)

This could be due to the increase of connectivity driving the glasses network to become more stressed rigid phase [62].

3.6. Correlation between structure and properties

In the present work, we did focus on the effect of the alumina content on T_g , elastic properties and the structure of the glasses. All system components do change with composition, which may explain the non-monotonic increase in the presented elastic properties. Also, the decrease of the ratio between CaO and Al_2O_3 induces a change in the role of Ca^{2+} cations where they go from network modifiers to charge compensators.

Indeed, the glass structural data can be used to relate the modification in glass structure to both, the variations of the glass transition temperatures (T_g) and the change in the elastic properties. When Al_2O_3 is added in the glass network we did not observe any change in the bond length of $Si-O$, $Al-O$, and $Ca-O$ bonds as seen from the first peak of the partial RDFs, while the average bond length of the $O-O$ bond has changed as indicated previously. Furthermore, we did not observe any effect on coordination numbers of both network formers (Si, Al) as shown in Fig. 3. Moreover, as discussed earlier the presence of Ca atoms play a role of charge balancing but when they are present in excess, they start modifying the glass network by creating NBOs and FOs and then play a modifier role. We also observed that the amount of NBOs and FOs decreases when the amount of Al_2O_3 increases. Moreover, as seen in Fig. 10(c), a monotonic increase of the average coordination number of oxygen atoms occurs with increasing alumina content; oxygen atoms are surrounded by more cations in the CAS6 sample than in the CS sample.

There is an increase in T_g with adding alumina in the calcium silicate network ($CaSiO_3$), up to 30 mol% of alumina. This is in agreement with a random substitution of Si atoms by Al atoms in Q^4 sites [33] (see Fig. S1 supplementary materials). In such a replacement, the connection of the network is changed and we see an increase of T_g values. The

insertion of Al_2O_3 improves the structural constraints on the network due to the Si/Al disorder and the necessity to preserve a fully polymerized network which leads to an increase of the Young's and bulk moduli. The increase of T_g can thus be related simply to the increased network polymerization, also it can be related to an increase of AlO_4^{2-} units as well as to the appearance of oxygen triclusters and to the decrease of free oxygens, which indicates the higher degree of polymerization of the network. Fig. 13 presents snapshots taken from different compositions to show the effect of adding alumina on the structure of the glass. In fact, at low alumina content, the network is mainly based on SiO_4 tetrahedra, with dispersed AlO_4^- units. As the CaO content decreases and the alumina content increases, the structure of glasses become more rigid, due to the conversion of the cations of the network modifiers into charge compensating cations. The connectivity of the network increases and then more thermal energy is required for atomic motion at high temperatures. This explains why the melts are more viscous, which implies that T_g values are higher for these glasses as mentioned by Cormier et al. [37]. This effect becomes more important as the CaO content decreases, showing that the network becomes even more polymerized. Also, the separation of the network into two regions as mentioned above would result in a rigidity fluctuation in the glass network, which may also explain the nonmonotonic increase in the elastic moduli.

The calcium silicate in this study, have a chain-like structure build mainly on Q^2 silicon tetrahedra as presented in Fig. S1 supplementary materials, with the increase of alumina content in the glass, there is also an increase in Q^3 and Q^4 . This is another indication that the glass network becomes more polymerized. With the increase of the alumina content in the systems, it is expected that the glass network will be formed by rings rather than chains as in calcium silicate glass, this behaviour is illustrated in Fig. 11. The presence of 4-, 5-, and 6-membered rings increases with increases alumina.

With the addition of alumina, Al is preferentially localized in various depolymerized Q^n species and, conversely, the numbers of Si and

Al in Q^4 sites increase (see Fig. S1 b and c). The glass network thus becomes more connected and rigid, which increases T_g and elastic moduli. The distribution of Si and Al over Q^n species is more homogeneous and Al contributes to the formation of the network (see supplementary materials Fig. S1). Therefore, the simple Si/Al mixing may explain the increase in T_g and elastic moduli within the 5–30 mol% Al_2O_3 content as reported for low silica content aluminosilicate glasses [37,63].

4. Conclusion

Structural, thermodynamic and mechanical properties were computed using molecular dynamics simulations. Elastic properties were investigated using two approaches, the first one is based on the concept of energy minimization and the second one uses molecular dynamics at finite temperature. The glass transition temperature was characterized by referring to the concept of inherent structure energy given in the potential energy landscape developed by Stillinger.

Our simulation results are in a realistic agreement with available experimental data for both thermodynamic and structural properties. The predicted elastic properties agree with the conclusion that the addition of alumina into silicate glass causes an increase in elastic moduli. The change in the glass transition temperature and mechanical properties has been attributed to the structural change when alumina content increases. The results suggest that variation in the calculated T_g , elastic and structural properties was found to be due to the mixed former (Si/Al) effect due to the presence of aluminium as a network former, the transformation of calcium atoms from network modifier to charge compensator, increase of the degree of network polymerization, mainly due to the addition of alumina in the network. Moreover, the rigidity fluctuation in the glass network due to the separation of the glass network into two regions, which is a consequence of the violation of the aluminium avoidance principle, and an increase of the oxygen triclusters and AlO_5^- units as well as a decrease of the free oxygens. The insight obtained from our simulations, is one step toward a deeper understanding of the relationship between the structure, and elastic properties.

Declaration of Competing Interest

None.

Appendix A. Supplementary data

Supplementary data to this article can be found online at <https://doi.org/10.1016/j.jnoncrysol.2019.119470>.

References

- [1] S. Freiman, M. Singh, G.S. Fischman, R. Cook, *Global Roadmap for Ceramics and Glass Technology*, Wiley, 2007.
- [2] Y. Xiang, J. Du, M.M. Smedskjaer, J.C. Mauro, Structure and properties of sodium aluminosilicate glasses from molecular dynamics simulations, *J. Chem. Phys.* 139 (2013) 044507, <https://doi.org/10.1063/1.4816378>.
- [3] F.S. Shirazi, M. Mehrali, A.A. Oshkour, H.S.C. Metselaar, N.A. Kadri, N.A. Abu Osman, Mechanical and physical properties of calcium silicate/alumina composite for biomedical engineering applications, *J. Mech. Behav. Biomed. Mater.* 30 (2014) 168–175, <https://doi.org/10.1016/j.jmbmm.2013.10.024>.
- [4] P.K. Hung, L.T. Vinh, T.B. Van, N.V. Hong, N.V. Yen, Insight into dynamics and microstructure of aluminum-silicate melts from molecular dynamics simulation, *J. Non-Cryst. Solids* 462 (2017) 1–9, <https://doi.org/10.1016/j.jnoncrysol.2017.02.003>.
- [5] R. Mathew, B. Stevansson, M. Edén, Na/ca intermixing around silicate and phosphate groups in bioactive Phosphosilicate glasses revealed by heteronuclear solid-state NMR and molecular dynamics simulations, *J. Phys. Chem. B* 119 (2015) 5701–5715, <https://doi.org/10.1021/acs.jpcc.5b01130>.
- [6] M. Micoulaut, M. Malki, P. Simon, A. Canizares, On the rigid to floppy transitions in calcium silicate glasses from Raman scattering and cluster constraint analysis, *Philos. Mag.* 85 (2005) 3357–3378, <https://doi.org/10.1080/14786430500157029>.
- [7] B.T. Poe, P.F. McMillan, B. Cote, D. Massiot, J.-P. Coutures, Structure and dynamics in calcium aluminate liquids: high-temperature ^{27}Al NMR and Raman Spectroscopy, *J. Am. Ceram. Soc.* 77 (1994) 1832–1838, <https://doi.org/10.1111/j.1151-2916.1994.tb07058.x>.
- [8] L.G. Hwa, C.L. Lu, L.C. Liu, Elastic moduli of calcium aluminosilicate glasses studied by Brillouin scattering, *Mater. Res. Bull.* 35 (2000) 1285–1292, [https://doi.org/10.1016/S0025-5408\(00\)00317-2](https://doi.org/10.1016/S0025-5408(00)00317-2).
- [9] L. Cormier, D. Ghaleb, D.R. Neuville, J.M. Delaye, G. Calas, Chemical dependence of network topology of calcium aluminosilicate glasses: a computer simulation study, *J. Non-Cryst. Solids* 332 (2003) 255–270, <https://doi.org/10.1016/j.jnoncrysol.2003.09.012>.
- [10] W.H. Zachariassen, The atomic arrangement in glass, *J. Am. Chem. Soc.* 54 (1932) 3841–3851, <https://doi.org/10.1021/ja01349a006>.
- [11] L. Deng, J. Du, Development of effective empirical potentials for molecular dynamics simulations of the structures and properties of boroaluminosilicate glasses, *J. Non-Cryst. Solids* 453 (2016) 177–194, <https://doi.org/10.1016/j.jnoncrysol.2016.09.021>.
- [12] W. Loewenstein, The distribution of aluminum in the tetrahedra of silicates and aluminates, *Am. Mineral.* (1954), <https://doi.org/10.1002/anie.201004007>.
- [13] D.R. Neuville, L. Cormier, D. De Ligny, J. Roux, A.M. Flank, P. Lagarde, Environments around Al, Si, and Ca in aluminate and aluminosilicate melts by X-ray absorption spectroscopy at high temperature, *Am. Mineral.* 93 (2008) 228–234, <https://doi.org/10.2138/am.2008.2646>.
- [14] J.F. Stebbins, E.V. Dubinsky, K. Kanehashi, K.E. Kelsey, Temperature effects on non-bridging oxygen and aluminum coordination number in calcium aluminosilicate glasses and melts, *Geochim. Cosmochim. Acta* 72 (2008) 910–925.
- [15] B.O. Mysrn, Role of Al in depolymerized, peralkaline aluminosilicate melts in the systems $Li_2O-Al_2O_3-SiO_2$, $Na_2O-Al_2O_3-SiO_2$, and $K_2O-Al_2O_3-SiO_2$, *Am. Mineral.* 75 (1990) 120–134.
- [16] D.R. Neuville, L. Cormier, D. Massiot, Al environment in tectosilicate and per-aluminous glasses: a ^{27}Al MQ-MAS NMR, Raman, and XANES investigation, *Geochim. Cosmochim. Acta* 68 (2004) 5071–5079, <https://doi.org/10.1016/j.gca.2004.05.048>.
- [17] M. Bauchy, Structural, vibrational, and elastic properties of a calcium aluminosilicate glass from molecular dynamics simulations: the role of the potential, *J. Chem. Phys.* 141 (2014) 024507, <https://doi.org/10.1063/1.4886421>.
- [18] N. Jakse, M. Bouhadja, J. Kozaily, J.W.E. Drewitt, L. Hennet, D.R. Neuville, H.E. Fischer, V. Cristiglio, A. Pasturel, Interplay between non-bridging oxygen, triclusters, and fivefold Al coordination in low silica content calcium aluminosilicate melts, *Appl. Phys. Lett.* 101 (2012) 201903, <https://doi.org/10.1063/1.4766920>.
- [19] M.J. Abdolhosseini Qomi, D. Ebrahimi, M. Bauchy, R. Pellenq, F.-J. Ulm, Methodology for estimation of nanoscale hardness via atomistic simulations, *J. Nanomechanics Micromechanics*. 7 (2017) 04017011, [https://doi.org/10.1061/\(ASCE\)NM.2153-5477.0000127](https://doi.org/10.1061/(ASCE)NM.2153-5477.0000127).
- [20] A. Hasnaoui, H. Van Swygenhoven, P.M. Derlet, Dimples on nanocrystalline fracture surfaces as evidence for shear plane formation, *Science* 300 (2003) 1550–1552, <https://doi.org/10.1126/science.1084284> (80-).
- [21] H. Van Swygenhoven, P.M. Derlet, A. Hasnaoui, Atomistic modeling of strength of nanocrystalline metals, *Adv. Eng. Mater.* 5 (2003) 345–350, <https://doi.org/10.1002/adem.200310080>.
- [22] M. Bouhadja, N. Jakse, A. Pasturel, Striking role of non-bridging oxygen on glass transition temperature of calcium aluminosilicate glass-formers, *J. Chem. Phys.* 140 (2014), <https://doi.org/10.1063/1.4882283>.
- [23] S. Plimpton, Fast parallel algorithms for short-range molecular dynamics, *J. Comput. Phys.* 117 (1995) 1–19, <https://doi.org/10.1006/jcph.1995.1039>.
- [24] S. Takahashi, D.R. Neuville, H. Takebe, Thermal properties, density and structure of percalcic and peraluminous $CaO-Al_2O_3-SiO_2$ glasses, *J. Non-Cryst. Solids* 411 (2015) 5–12, <https://doi.org/10.1016/j.jnoncrysol.2014.12.019>.
- [25] A. Pedone, G. Malavasi, M. Cristina Menziani, U. Segre, A.N. Cormack, Molecular dynamics studies of stress-strain behavior of silica glass under a tensile load, *Chem. Mater.* 20 (2008) 4356–4366, <https://doi.org/10.1021/cm800413v>.
- [26] X. Li, W. Song, K. Yang, N.M.A. Krishnan, B. Wang, M.M. Smedskjaer, J.C. Mauro, G. Sant, M. Balonis, M. Bauchy, Cooling rate effects in sodium silicate glasses: bridging the gap between molecular dynamics simulations and experiments, *J. Chem. Phys.* 147 (2017) 074501, <https://doi.org/10.1063/1.4998611>.
- [27] F.H. Stillinger, A topographic view of supercooled liquids and glass formation, *Science* (80-) 267 (1995) 1935–1939, <https://doi.org/10.1126/science.267.5206.1935>.
- [28] F.H. Stillinger, Supercooled liquids and the glass transition, *Nature, WORLD SCIENTIFIC*, 2001, p. 259, https://doi.org/10.1142/9789814273459_0005.
- [29] D.J. Wales, *Energy Landscapes*, Cambridge University Press, 2003.
- [30] T. Schneider, E. Stoll, Molecular-dynamics study of a three-dimensional one-component model for distortive phase transitions, *Phys. Rev. B* 17 (1978) 1302–1322, <https://doi.org/10.1103/PhysRevB.17.1302>.
- [31] R. Chibante, *Simulated Annealing, Theory with Applications*, Sciyo, 2010.
- [32] E.D. Zanotto, J.C. Mauro, The glassy state of matter: its definition and ultimate fate, *J. Non-Cryst. Solids* 471 (2017) 490–495, <https://doi.org/10.1016/j.jnoncrysol.2017.05.019>.
- [33] L. Cormier, D.R. Neuville, G. Calas, Structure and properties of low-silica calcium aluminosilicate glasses, *J. Non-Cryst. Solids* 274 (2000) 110–114, [https://doi.org/10.1016/S0022-3093\(00\)00209-X](https://doi.org/10.1016/S0022-3093(00)00209-X).
- [34] C.W. Burnham, M.J. Buerger, Refinement of the crystal structure of andalusite, *Zeitschrift Für Krist.* 115 (1961) 269–290, <https://doi.org/10.1524/zkri.1961.115.3-4.269>.
- [35] N. Ishizawa, T. Miyata, I. Minato, F. Marumo, S. Iwai, A structural investigation of $\alpha-Al_2O_3$ at 2170 K, *Acta Crystallogr. Sect. B Struct. Crystallogr. Cryst. Chem.* 36

- (1980) 228–230, <https://doi.org/10.1107/S0567740880002981>.
- [36] R.-S. Zhou, R.L. Snyder, Structures and transformation mechanisms of the η , γ and θ transition aluminas, *Acta Crystallogr. Sect. B*. 47 (1991) 617–630, <https://doi.org/10.1107/S0108768191002719>.
- [37] L. Cormier, D.R. Neuville, G. Calas, Relationship between structure and glass transition temperature in low-silica calcium aluminosilicate glasses: the origin of the anomaly at low silica content, *J. Am. Ceram. Soc.* 88 (2005) 2292–2299, <https://doi.org/10.1111/j.1551-2916.2005.00428.x>.
- [38] P.H. Gaskell, M.C. Eckersley, A.C. Barnes, P. Chieux, Medium-range order in the cation distribution of a calcium silicate glass, *Nature*. 350 (1991) 675–677, <https://doi.org/10.1038/350675a0>.
- [39] M.C. Abramo, C. Caccamo, G. Pizzimenti, Structural properties and medium-range order in calcium-metasilicate (CaSiO₃) glass: a molecular dynamics study, *J. Chem. Phys.* 96 (1992) 9083–9091, <https://doi.org/10.1063/1.462217>.
- [40] H. Jabraoui, M. Malki, A. Hasnaoui, M. Badawi, S. Ouaskit, S. Lebègue, Y. Vaills, Thermodynamic and structural properties of binary calcium silicate glasses: insights from molecular dynamics, *Phys. Chem. Chem. Phys.* 19 (2017) 19083–19093, <https://doi.org/10.1039/c7cp03397d>.
- [41] Z. Yu, A. Zheng, Q. Wang, L. Chen, J. Xu, J.-P. Amoureux, F. Deng, Insights into the Dealumination of zeolite HY revealed by sensitivity-enhanced ²⁷Al DQ-MAS NMR spectroscopy at high field, *Angew. Chemie Int. Ed.* 49 (2010) 8657–8661, <https://doi.org/10.1002/anie.201004007>.
- [42] A.R. Allu, A. Gaddam, S. Ganiseti, S. Balaji, R. Siegel, G.C. Mather, M. Fabian, M.J. Pascual, N. Ditaranto, W. Milius, J. Senker, D.A. Agarkov, V.V. Kharton, J.M.F. Ferreira, Structure and crystallization of alkaline-earth Aluminosilicate glasses: prevention of the alumina-avoidance principle, *J. Phys. Chem. B* 122 (2018) 4737–4747, <https://doi.org/10.1021/acs.jpcc.8b01811>.
- [43] P. Ganster, M. Benoit, W. Kob, J.-M. Delaye, Structural properties of a calcium aluminosilicate glass from molecular-dynamics simulations: a finite size effects study, *J. Chem. Phys.* 120 (2004) 10172–10181, <https://doi.org/10.1063/1.1724815>.
- [44] L. Mongalo, A.S. Lopis, G.A. Venter, Molecular dynamics simulations of the structural properties and electrical conductivities of CaO–MgO–Al₂O₃–SiO₂ melts, *J. Non-Cryst. Solids* 452 (2016) 194–202, <https://doi.org/10.1016/j.jnoncrysol.2016.08.042>.
- [45] J.F. Stebbins, Z. Xu, NMR evidence for excess non-bridging oxygen in an aluminosilicate glass, *Nature*. 390 (1997) 60–62, <https://doi.org/10.1038/36312>.
- [46] T.K. Bechgaard, G. Scannell, L. Huang, R.E. Youngman, J.C. Mauro, M.M. Smedskjaer, Structure of MgO/CaO sodium aluminosilicate glasses: Raman spectroscopy study, *J. Non-Cryst. Solids* 470 (2017) 0–1, <https://doi.org/10.1016/j.jnoncrysol.2017.05.014>.
- [47] R.G. Kuryaeva, Degree of polymerization of aluminosilicate glasses and melts, *Glas. Phys. Chem.* 30 (2004) 157–166, <https://doi.org/10.1023/B:GPAC.0000024000.19443.f6>.
- [48] R.G. Kuryaeva, Degree of polymerization of the CaAl₂Si₂O₈ aluminosilicate glass, *Glas. Phys. Chem.* 30 (2004) 157–166, <https://doi.org/10.1023/B:GPAC.0000024000.19443.f6>.
- [49] S. Le Roux, P. Jund, Ring statistics analysis of topological networks: new approach and application to amorphous GeS₂ and SiO₂ systems, *Comput. Mater. Sci.* 49 (2010) 70–83, <https://doi.org/10.1016/j.commatsci.2010.04.023>.
- [50] A. Pönitzsch, M. Nofz, L. Wondraczek, J. Deubener, Bulk elastic properties, hardness and fatigue of calcium aluminosilicate glasses in the intermediate-silica range, *J. Non-Cryst. Solids* 434 (2016) 1–12, <https://doi.org/10.1016/j.jnoncrysol.2015.12.002>.
- [51] N.P. Bansal, R.H. Doremus, *Handbook of Glass Properties*, Academic Press, 2013, <https://doi.org/10.1016/C2009-0-21785-5>.
- [52] B. Stevansson, M. Edén, Structural rationalization of the microhardness trends of rare-earth aluminosilicate glasses: interplay between the RE³⁺ field-strength and the aluminum coordinations, *J. Non-Cryst. Solids* 378 (2013) 163–167, <https://doi.org/10.1016/j.jnoncrysol.2013.06.013>.
- [53] J. Johnson, R. Weber, M. Grimsditch, Thermal and mechanical properties of rare earth aluminate and low-silica aluminosilicate optical glasses, *J. Non-Cryst. Solids* 351 (2005) 650–655, <https://doi.org/10.1016/j.jnoncrysol.2005.01.065>.
- [54] A. Rosenflanz, M. Frey, B. Endres, T. Anderson, E. Richards, C. Schardt, Bulk glasses and ultrahard nanoceramics based on alumina and rare-earth oxides, *Nature*. 430 (2004) 761–764, <https://doi.org/10.1038/nature02729>.
- [55] B. Pahari, S. Iftekhhar, A. Jaworski, K. Okhotnikov, K. Jansson, B. Stevansson, J. Grins, M. Edén, Composition-property-structure correlations of scandium aluminosilicate glasses revealed by multinuclear ⁴⁵Sc, ²⁷Al, and ²⁹Si solid-state NMR, *J. Am. Ceram. Soc.* 95 (2012) 2545–2553, <https://doi.org/10.1111/j.1551-2916.2012.05288.x>.
- [56] S. Tanabe, K. Hirao, N. Soga, Elastic properties and molar volume of rare-earth aluminosilicate glasses, *J. Am. Ceram. Soc.* 75 (1992) 503–506, <https://doi.org/10.1111/j.1151-2916.1992.tb07833.x>.
- [57] J. Sehgal, S. Ito, A new low-brittleness glass in the soda – lime – silica glass family, *J. Am. Ceram. Soc.* 81 (1998) 2485–2488, <https://doi.org/10.1111/j.1151-2916.1998.tb02649.x>.
- [58] T.M. Gross, M. Tomozawa, A. Koike, A glass with high crack initiation load: role of fictive temperature-independent mechanical properties, *J. Non-Cryst. Solids* 355 (2009) 563–568, <https://doi.org/10.1016/j.jnoncrysol.2009.01.022>.
- [59] H. Morozumi, H. Nakano, S. Yoshida, J. Matsuoka, Crack initiation tendency of chemically strengthened glasses, *Int. J. Appl. Glas. Sci.* 6 (2015) 64–71, <https://doi.org/10.1111/ijag.12089>.
- [60] Y. Kato, H. Yamazaki, S. Yoshida, J. Matsuoka, Effect of densification on crack initiation under Vickers indentation test, *J. Non-Cryst. Solids* 356 (2010) 1768–1773, <https://doi.org/10.1016/j.jnoncrysol.2010.07.015>.
- [61] P. Sellappan, T. Rouxel, F. Celarie, E. Becker, P. Houzot, R. Conradt, Composition dependence of indentation deformation and indentation cracking in glass, *Acta Mater.* 61 (2013) 5949–5965, <https://doi.org/10.1016/j.actamat.2013.06.034>.
- [62] A. Sharma, A.J. Licup, K.A. Jansen, R. Rens, M. Sheinman, G.H. Koenderink, F.C. MacKintosh, Strain-controlled criticality governs the nonlinear mechanics of fibre networks, *Nat. Phys.* 12 (2016) 584–587, <https://doi.org/10.1038/nphys3628>.
- [63] G.A. Rosales-Sosa, A. Masuno, Y. Higo, H. Inoue, Crack-resistant Al₂O₃–SiO₂ glasses, *Sci. Rep.* 6 (2016) 23620, <https://doi.org/10.1038/srep23620>.